Journal of Catalysis 285 (2012) 134–144

Contents lists available at SciVerse ScienceDirect

Journal of Catalysis

journal homepage: www.elsevier.com/locate/jcat

Potassium-modified molybdenum-containing SBA-15 catalysts for highly efficient production of acetaldehyde and ethylene by the selective oxidation of ethane

Jian Liu [a], Lihong Yu [a], Zhen Zhao [a,*], Yongsheng Chen [b,*], Pengyu Zhu [b], Chao Wang [a], Yan Luo [a], Chunming Xu [a], Aijun Duan [a], Guiyuan Jiang [a]

[a] State Key Laboratory of Heavy Oil, College of Science, China University of Petroleum, Beijing 102249, People's Republic of China
[b] EMS Energy Institute and John and Willie Leone Family Department of Energy and Mineral Engineering, The Pennsylvania State University, University Park, PA 16802, USA

ARTICLE INFO

Article history:
Received 2 April 2011
Revised 21 September 2011
Accepted 22 September 2011
Available online 29 November 2011

Keywords:
Selective oxidation of ethane
Molybdenum
Molybdenum-containing SBA-15
Highly dispersed and isolated MoO_x species
Catalysts
Kinetics

ABSTRACT

Mo-incorporated SBA-15 (Mo-SBA-15) catalysts with different Mo:Si molar ratios were synthesized by a direct hydrothermal method, and SBA-15-supported Mo catalysts (Mo/SBA-15 and K-Mo/SBA-15) were prepared by an incipient-wetness impregnation method. The structures of the catalysts were characterized by means of N_2 adsorption–desorption, XRD, TEM, FT-IR, and UV-Raman, and their catalytic performance for the oxidation of ethane was tested. Turnover frequency and product selectivity are strongly dependent on the molybdenum content and catalyst preparation method. Furthermore, the addition of potassium promotes the formation of isolated tetra-coordination molybdenum species and potassium molybdate. The K/Mo-SBA-15 catalysts possess much higher catalytic selectivity to acetaldehyde in the selective oxidation of ethane than the supported molybdenum catalysts (Mo/SBA-15 or K-Mo/SBA-15). The highest selectivity of $CH_3CHO + C_2H_4$ 68.3% is obtained over the K/Mo-SBA-15 catalyst. Analysis of kinetic results supports the conclusion that ethane oxidation is the first-order reaction and ethane activation may be the rate-determining step for the oxidation of ethane. Ethylene is a possible intermediate for acetaldehyde formation.

1. Introduction

One of the major challenges for the petrochemical industry is to manufacture valuable products by oxidizing lower alkanes instead of olefins or aromatics for effective utilization of abundant natural gas resources. The direct transformation of methane and ethane to useful olefins and oxygenates has attracted much attention from chemists and chemical engineers. Compared with the processes of naphtha oxidation and methanol carbonylation (currently used to obtain acetic acid), direct selective oxidation of ethane is more attractive for easier separation of products and lower cost of ethane [1]. Usually, high temperatures (>500 °C) are required for the conversion of ethane because of the low reactivity of its C—H bonds [2]. However, valuable oxygenates formed may be instantly converted to CO and CO_2 under such conditions. Thus, selective oxidation of ethane to oxygenates is very difficult, and it is not an easy task to obtain oxygenates with one-pass yields higher than 4%, even if N_2O is used as a selective oxidant [2–4]. Although many attempts at partial oxidation of ethane have been reported, viable processes and effective catalysts have not been developed.

A variety of catalysts for the selective oxidation of ethane have been examined. Vanadium- [5–7] and molybdenum- [3,8,9] based catalysts have been widely studied in the selective oxidation of alkanes. For example, Wang et al. found a new route for the selective oxidation of ethane to formaldehyde and acetaldehyde over SBA-15-supported molybdenum catalysts [3], and Corberan et al. prepared a novel V-UVM-7 bimodal mesoporous catalyst for the selective oxidative activation of isobutane and obtained a high selectivity of isobutene, 42.6% [10]. The performance of these catalysts is strongly related to the nature of the active species. It has been reported that isolated vanadium or molybdenum species with low aggregation and/or coordination structure favor the selective formation of oxygenates, whereas polymeric species or crystalline MoO_x species are suitable for deep oxidation of alkanes [4,11,12]. In the past decades, highly dispersed catalysts with isolated active sites have been developed, which may avoid overoxidation of the partially oxidized products to undesired carbon oxides [4,7–12]. Moreover, the activity and the selectivity of the catalysts also seem to depend on the nature of the support, and pure silica materials with weak surface acidity are favorable for the oxidation of alkanes to oxygenates. Mesoporous molecular sieves, MCM-41 and SBA-15,

* Corresponding authors.
E-mail addresses: zhenzhao@cup.edu.cn (Z. Zhao), yzc2@psu.edu (Y. Chen).

0021-9517/$ - see front matter © 2011 Elsevier Inc. All rights reserved.
doi:10.1016/j.jcat.2011.09.029

which have high surface area, large pore volume, regular structure, uniform pore size distribution, and relative high thermal stability, are preferred supports for catalyst preparation [13,14]. However, pure silica, SBA-15, shows very limited catalytic activity for its weak redox properties, basicity, and acidity. Therefore, it is necessary to introduce catalytic active sites into the framework of SBA-15 and to improve its catalytic activity. For instance, the incorporation of certain transition metal ions such as vanadium into the framework of mesoporous molecular sieves can produce catalysts with remarkable catalytic activity for many reactions [3,15]. The catalysts, which have dispersed active species and in which the active metals exist in a tetrahedral coordination structure, yield high selectivity to aldehyde. This kind of framework-incorporated catalysts is different from supported catalysts. The active metal ions are fully isolated and dispersed throughout the support, and therefore, high concentrations of active sites can be achieved in framework-incorporated catalysts. In contrast, in supported catalysts, the active phases are only present on the surface or in the pores of the support and may aggregate further. The use of vanadium incorporation into mesoporous silicon materials for the activation of lower alkanes with oxygen was recently reported [10,15], but molybdenum incorporation into mesoporous frameworks for the selective oxidation of lower alkanes has not been reported so far.

Alkali metals are another important component in the catalysts. In most cases, they are employed as promoters to improve the catalytic performance. In recent years, significant improvements in the catalytic performance of alkali metal-modified catalysts have been reported for several very important reactions [12,16–18]. The effect of alkali metal on the physicochemical characteristics of catalysts commonly involves acid–base interaction, adsorption/desorption behavior, and the reducibility of the catalysts. The addition of alkali metals can reduce the acidity of the catalyst and increase the dispersion of the active sites [18]. All together, these functions can inhibit the excessive oxidation of oxygenate products and enhance the formation of aldehyde. Thus, the alkali metal-modified Mo-incorporated mesoporous sieves may be good catalysts for the selective oxidation of low alkanes.

In this work, we report the synthesis and catalytic behavior of a novel framework-incorporated Mo-containing SBA-15 mesoporous mixed oxide, denoted as Mo-SBA-15, for the selective oxidation of ethane. The effects of the preparation method and the presence/absence of potassium on the structure of MoO_x in the Mo-containing SBA-15 catalysts are investigated, and their catalytic performance for the oxidation of ethane is compared. The kinetic analysis and reaction pathways on the best K/Mo-SBA-15 catalysts are also preliminarily discussed.

Table 2
Physical properties of Mo/SBA-15 and K-Mo/SBA-15 catalysts with different Mo contents.

Sample	Mo:Si:molar ratio	S_{BET}, m^2 g	V_p, cm^3 g	D, nm
I0.1	0.0025:100	497.8	0.87	6.99
I2.5	0.038:100	476.9	0.85	7.16
I5	0.045:100	466.4	0.84	7.18
I8	0.13:100	442.9	0.78	7.05
I10	1.85:100	383.5	0.75	7.82
I12	6.79:100	355.4	0.65	7.37
IK0.1	0.0025:100			
IK2.5	0.038:100	396.7	0.75	7.60
IK5	0.045:100	397.7	0.75	7.59
IK8	0.13:100	398.4	0.73	7.35
IK10	1.85:100	331.0	0.62	7.51
IK12	6.79:100	135.4	0.51	15.21

Notes: F is denoted as framework-incorporation sample Mo-SBA-15; I is denoted as incipient-wetness impregnation sample Mo/SBA-15; FK is denoted as the K/Mo-SBA-15 sample after potassium was impregnated on Mo-SBA-15; IK is denoted as the K-Mo/SBA-15 sample after potassium was further impregnated on Mo/SBA-15.

2. Experimental

2.1. Catalyst preparation

Mo-incorporated mesoporous molecular sieves, Mo-SBA-15, were synthesized by the direct hydrothermal (DHT) method using tetraethyl orthosilicate (TEOS) and ammonium molybdate ($(NH_4)_6Mo_7O_{24}{\cdot}4H_2O$) as starting materials. Nonionic triblock copolymer surfactant, $EO_{20}PO_{70}EO_{20}$ (P123, Aldrich, analytic grade), was used as the structure-directing agent. The typical preparation procedure of Mo-SBA-15 materials is described as follows. A quantity of 8 g of P123 was dissolved in 240 mL HCl to form a solution (denoted as "solution A"). A certain amount of ammonium molybdate (the initial molar ratio of Mo to Si was 0.001, 0.025, 0.05, 0.08, 0.10, or 0.12) was dissolved in 60 mL of deionized water, and the solution was stirred at room temperature for about 10 min and then added into solution A. The resulting solution was heated to 40 °C and kept at that temperature for 4 h while being stirred. Subsequently, 17 g TEOS was gradually added to the solution and continuously stirred for 4 h. A small amount of aqueous ammonia was then added to the solution to adjust the pH value to 3. The solution was stirred at 40 °C for 24 h. The resulting gel was placed in a Teflon autoclave and maintained at 100 °C for 48 h. The solid products were filtered, washed, and dried at 100 °C in air for 12 h and calcined at 600 °C for 4 h. In the filtration and washing processes, any Mo species that is not incorporated into the catalysts would be washed away. Finally, the mesoporous Mo-SBA-15 samples were obtained. The final Mo

Table 1
Physical properties of Mo-SBA-15 and K/Mo-SBA-15 catalysts with different Mo contents.

Sample	Mo:Si (in recipe)/molar ratio	Mo:Si(by XRF):molar ratio	2θ, ° (100)	d(100)	S_{BET}, m^2 g	V_p, cm^3 g	D, nm
SBA-15			0.837	10.6	849.5	1.21	5.68
F0.1	0.1:100	0.0025:100	0.797	11.1	915.1	1.26	5.52
F2.5	2.5:100	0.038:100	0.740	11.9	872.4	1.27	5.84
F5	5:100	0.045:100	0.820	10.8	776.9	1.10	5.66
F8	8:100	0.13:100	0.819	10.7	837.5	1.15	5.47
F10	10:100	1.85:100	0.800	11.0	640.9	0.93	5.80
F12	12:100	6.79:100	–	–	382.9	0.71	7.37
FK0.1	0.5:0.1:100	0.5:0.0025:100	0.900	9.8	415.3	0.77	7.40
FK2.5	0.5:2.5:100	0.5:0.038:100	0.919	9.6	403.2	0.72	7.12
FK5	0.5:5:100	0.5:0.045:100	0.879	11.0	375.9	0.67	7.08
FK8	0.5:8:100	0.5:0.13:100	0.920	9.6	325.4	0.57	6.85
FK10	0.5:10:100	0.5:1.85:100	0.880	10.0	285.5	0.46	6.48
FK12	0.5:12:100	0.5:6.79:100			52.3	0.16	11.90

Notes: F is denoted as framework-incorporation sample Mo-SBA-15; I is denoted as incipient-wetness impregnation sample Mo/SBA-15; FK is denoted as the K/Mo-SBA-15 sample after potassium was impregnated on Mo-SBA-15; IK is denoted as the K-Mo/SBA-15 sample after potassium was further impregnated on Mo/SBA-15.

contents in Mo-SBA-15 samples were determined by X-ray fluorescence (XRF) measurement.

In addition, supported molybdenum and potassium–molybdenum catalysts including Mo/SBA-15, K-Mo/SBA-15, and K/Mo-SBA-15 samples were prepared by the incipient-wetness impregnation method using ammonium molybdate and/or KNO_3 aqueous solution as Mo and/or K precursors. The amount of $(NH_4)_6Mo_7O_{24}{\cdot}4H_2O$ was varied in order to achieve different Mo-to-Si ratios ranging from 0.001 to 0.12, and whenever potassium was added, the molar ratio between K and Si was kept at 0.005. The samples were dried at 100 °C for 6 h and then calcined at 600 °C for 4 h in air. In this work, all chemical reagents except P123 were purchased from Beijing Chemical Reagent Company in China and were of analytic grade. For the sake of brevity, the catalysts are named F, I, FK, and IK in the tables and figures. F denotes framework-incorporated sample Mo-SBA-15; I denotes incipient-wetness impregnation sample Mo/SBA-15; FK denotes the K/Mo-SBA-15 sample after potassium was impregnated on Mo-SBA-15; and IK denotes the K-Mo/SBA-15 sample after potassium was further impregnated on Mo/SBA-15.

2.2. Catalyst characterization

Nitrogen adsorption/desorption isotherms at −196 °C were recorded using a Micromeritics ASAP 2010 porosimeter. The samples were outgassed in N_2 flow at 80 °C for 4 h before the measurements. X-ray fluorescence (XRF) measurements were taken on a CSX-1000E spectrometer. Low-angle X-ray diffraction (XRD) patterns were collected on a SIEMENS D5000 diffractometer in a 2θ range from 0.7° to 10° with a step size of 0.02°. Transmission electron microscopy (TEM) images were taken on a JEM-200CX instrument at an acceleration voltage of 200 kV. The TEM samples were sonicated and well suspended in ethanol. Drops of the suspension were applied, and after drying, the fine particles were well dispersed on a copper grid coated with carbon. Fourier transform infrared spectra (FT-IR) were collected on a FTS-3000 IR instrument running at 2 cm^{-1} resolution. The samples were mixed with KBr (sample:KBr = 1:100 mass ratio) and pressed into pellets. The spectra were collected in the range of 4000 to 400 cm^{-1}, and KBr was used as background. UV-Raman spectra were obtained on a LabRAM HR spectrometer (Horiba Jobin Yvon). The laser wavelength was 325 nm. A laser power of 0.2 mW was applied at the sample.

2.3. Catalytic activity measurements

The catalytic reactions were carried out in a fixed-bed flow reactor at atmospheric pressure. A quantity of 300 mg of the catalyst was charged into the reactor. The catalyst particle size was in the range 0.4–0.5 mm. The catalyst was pretreated in the quartz reactor (6 mm i.d., 400 mm length) with a gas flow containing high-purity N_2 and O_2 at 575 °C for 30 min, followed by purging with high-purity N_2 at the same temperature. The reactant gas mixture, consisting of ethane and oxygen (C_2H_6/O_2 = 3:1), was passed through the catalyst bed (maintained at 575 °C) at a flow rate of 15 ml min^{-1}. All reactant gases were purchased from the Dalian Date Standard Gas Company in China, and the purity was greater than 99.999%. To accurately detect the true reaction temperature, the catalyst bed was sandwiched between two quartz-wool layers, and the tip of a K-type thermocouple was inserted into the catalyst bed. The reaction temperature was controlled through a PID-regulation system based on the measurements of an external K-type thermocouple. The height of the catalyst bed was about 30 mm, and the length of the isothermal zone of the reactor oven was 60 mm. The reaction space velocity (GHSV) was about 3200 h^{-1}. The reaction products were analyzed by online gas chromatography (GC) (SP3420, Beijing, People's Republic of China) equipped with two flame ionization detectors (FID) and two methane converters operating at 380 °C using a Ni catalyst. All lines and valves between the exit of the reactor and the GC were kept at 120 °C to prevent condensation of the products. C_2H_6, C_2H_4, and organic oxygenates in the products, including CH_3CHO and acrolein, were separated in a Porapak Q column. Separation of other components, such as HCHO, CH_4, CO, and CO_2, was carried out in a TDX-01 column.

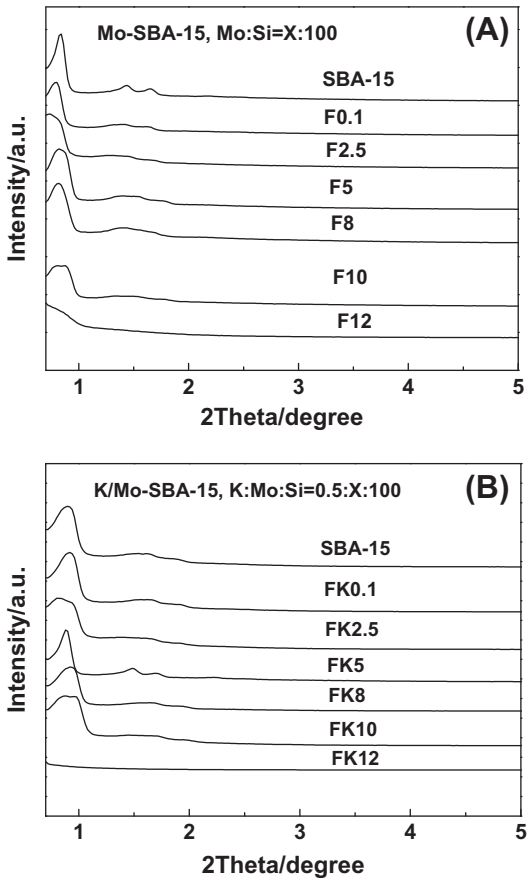

Fig. 1. Low-angle powder XRD patterns of Mo-SBA-15 and K/Mo-SBA-15 samples with different Mo:Si molar ratios.

3. Results and discussion

3.1. Structural characterization of the materials

The Mo content of Mo-SBA-15 and K/Mo-SBA-15 catalysts was determined by XRF and is presented in Table 1. The final Mo content in each catalyst is very different from what was used in the recipe, indicating that a large amount of Mo was not incorporated into the framework of SBA-15. Therefore, when preparing the SBA-15 supported catalysts (Mo/SBA-15 and K-Mo/SBA-15 samples), we used the corresponding XRF-determined Mo contents in the Mo-SBA-15 samples. Physical properties of the incorporated and supported catalysts are reported in Tables 1 and 2, respectively. For the samples with the highest Mo loading (nominal Mo content x = 12), relatively more Mo remains in the catalysts. This might be due to the collapse of the mesoporous structure of SBA-15 and the formation of nanoparticle MoO_x species on these catalysts. Thus, the growth of crystal MoO_x species inside the mesoporous channels destroys the silica wall of SBA-15 [3].

The XRD patterns in the range $0.5° < 2\theta < 5°$ of the Mo-SBA-15 and K/Mo-SBA-15 samples with different Mo:Si molar ratios are shown in Fig. 1. The DHT samples with various Mo contents exhibit a sharp peak at about 0.8° and two weak peaks at 1.4° and 1.6°, corresponding to the (100), (110), and (200) planes in SBA-15, which are the characteristics of mesoporous material with a space group of P6 mm symmetry [13]. This confirms the formation of the highly ordered 2D-hexagonal P6 mm structure. As Mo content increases to $x = 12$, these characteristic peaks almost disappear whether potassium is present or not, indicating a decrease in structural regularity. Moreover, as shown in Table 1, the d spacing between (100) planes in the Mo-loaded catalysts is larger than that in the pure siliceous SBA-15, suggesting the incorporation of Mo into the framework of SBA-15. This is probably because the partial substitution of the larger Mo ion for Si results in the expansion of the crystal structure of SBA-15. Moreover, the addition of potassium seems to reduce the (100) d spacing in all samples except FK5. This clearly shows that the introduction of potassium affects the structures of the catalysts.

To gain more insight into the structure of DHT catalysts, morphologies of the Mo-SBA-15 and K/Mo-SBA-15 catalysts were examined by TEM. Fig. 2 shows TEM micrographs of typical Mo-SBA-15 and K/Mo-SBA-15 samples. When the molar ratio of Mo to Si is equal to 0.1 or 10, the TEM images show well-ordered hexagonal arrays of mesopores with one-dimensional channels, manifesting a P6 mm mesoporous structure. The hexagonal arrays of mesopores with one-dimensional channels are partially maintained in the F12 catalyst. However, the order of the mesoporous structure has been destroyed. The addition of potassium causes the partial collapse of the mesoporous structure in FK12.

Nitrogen adsorption–desorption isotherms for the catalysts synthesized by different methods are presented in Fig. 3, and their

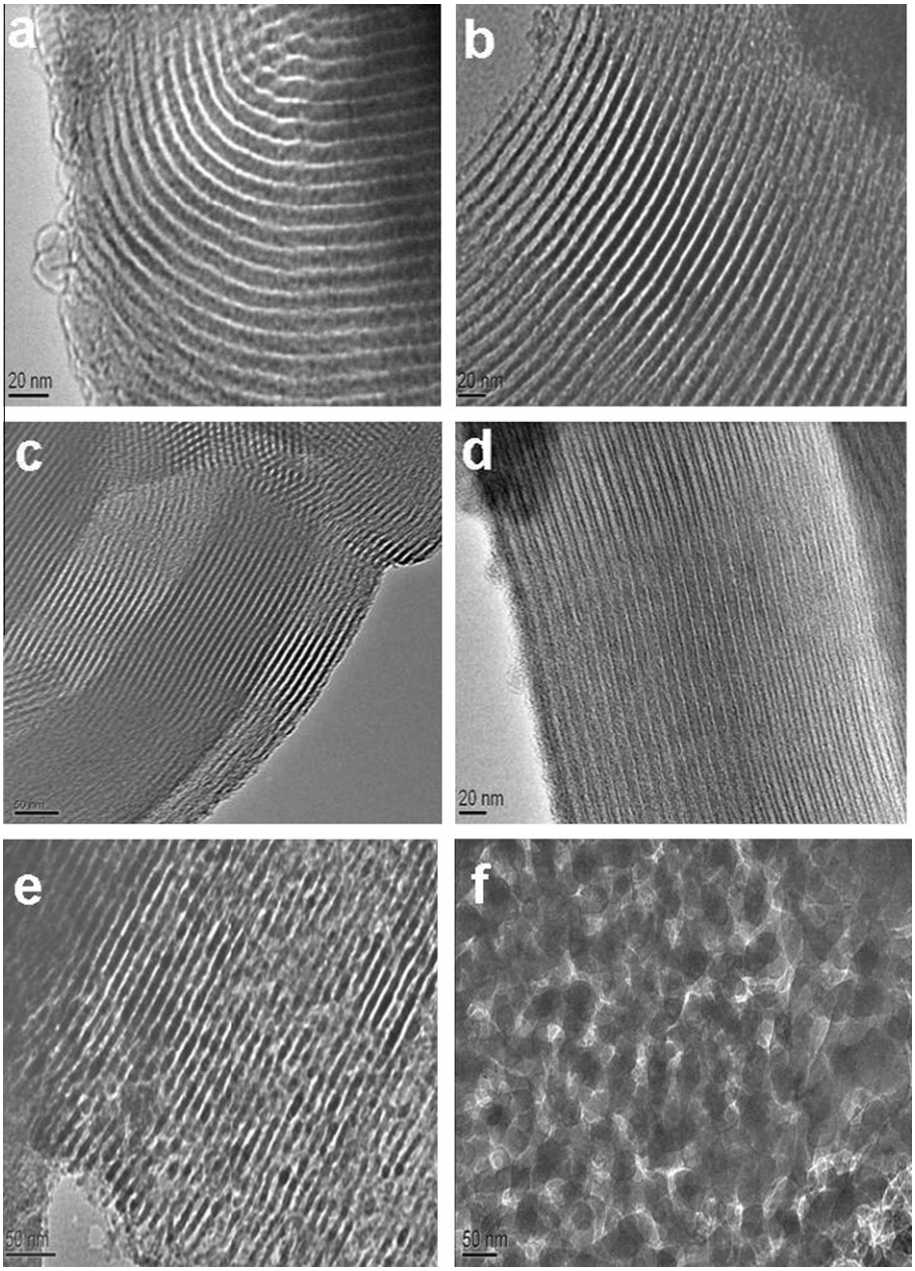

Fig. 2. TEM images of Mo-SBA-15 and K/Mo-SBA-15. (a) Mo-SBA-15, Mo:Si = 0.1:100; (b) K/Mo-SBA-15, K:Mo:Si = 0.5:0.1:100; (c) Mo-SBA-15, Mo:Si = 10:100; (d) K/Mo-SBA-15, K:Mo:Si = 0.5:10:100; (e) Mo-SBA-15, Mo:Si = 12:100; (f) K/Mo-SBA-15, K:Mo:Si = 0.5:12:100.

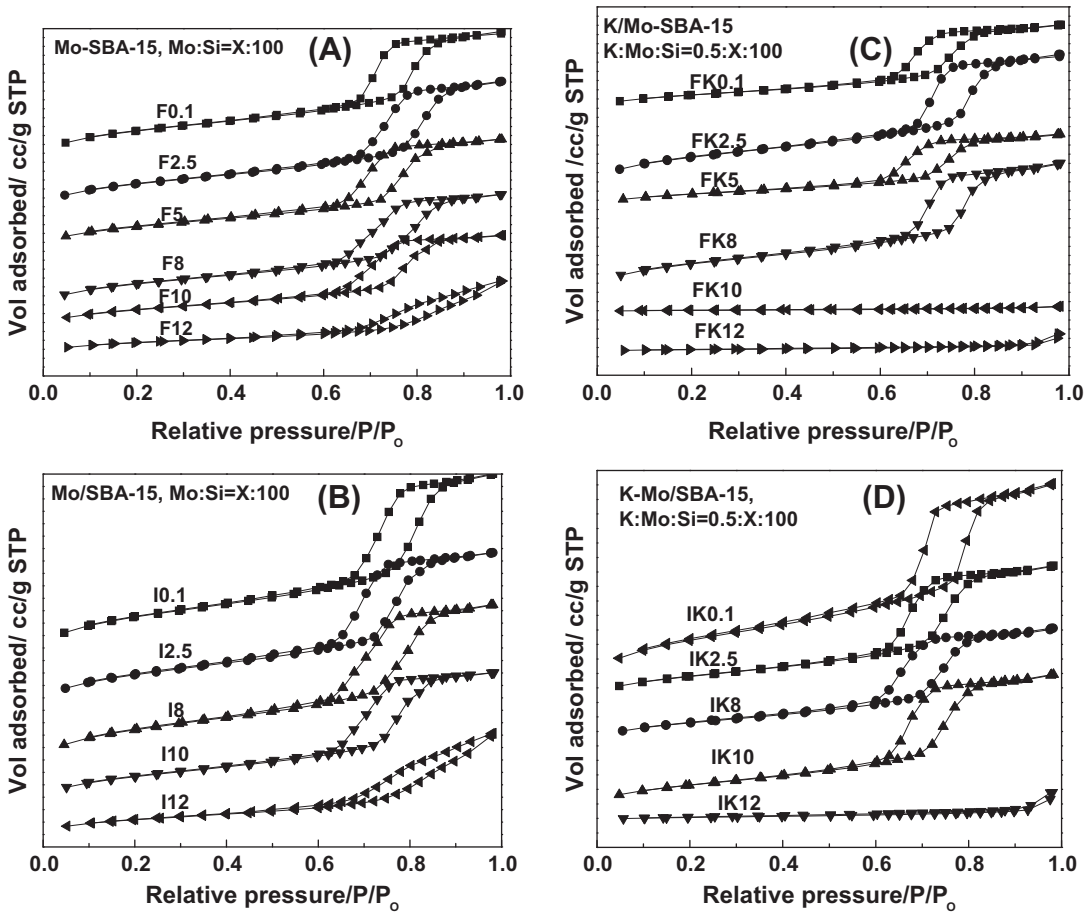

Fig. 3. Nitrogen adsorption–desorption isotherms of catalysts with different Mo:Si molar ratios. (A) Mo-SBA-15; (B) Mo/SBA-15; (C) K/Mo-SBA-15; (D) K-Mo/SBA-15.

physical properties are presented in Tables 1 and 2. The DHT and IWI catalysts have similar textural properties. The isotherms of the catalysts with low Mo content are of type IV with an H1 hysteresis loop, showing typical characteristics for mesoporous materials with a 2D-hexagonal structure [13]. A general trend of decreasing pore volume is observed with increasing Mo loading. A dramatic decrease in pore volume with high Mo loading, as in FK12, is noticed. Moreover, the surface area of the K-modified sample is remarkably lower than that of the corresponding Mo-SBA-15 catalyst when the Mo content is the same. This may be due to the introduction of K blocking up the mesoporous channel of SBA-15. The introduction of K plays a major role in the K/Mo-SBA-15 catalysts; their surface areas, in fact, look closer to those of the catalysts prepared by incipient-wetness impregnation. However, Mo is incorporated into the framework of SBA-15 and does not occupy the pore channels of SBA-15 for the Mo-SBA-15 catalysts. Therefore, the introduction of Mo only slightly affects the surface areas of catalysts. Thus, the difference in the surface area of catalysts doped with K and Mo may suggest that Mo should be incorporated into the framework of SBA-15.

The FT-IR spectra of the DHT and the IWI catalysts are shown in Fig. 4. Two characteristic bands at ~463 and ~802 cm^{-1} can be detected in all samples. The band centered at 463 cm^{-1} is assigned to the flexural vibrations of Si–O–Si, and the band centered at about 802 cm^{-1} is ascribed to the symmetric stretching vibration of tetrahedral SiO_4 [19–22]. In Fig. 4A, the band at 953 cm^{-1} can be assigned to the stretching vibration mode of an [SiO_4] unit bonded to a heteroatom (Si–O–M) in silicate molecular sieves [23], suggesting the incorporation of Mo into the framework of molecular sieves in the DHT Mo-SBA-15 catalysts. However, this band at 953 cm^{-1} is not detected for the IWI Mo/SBA-15 samples, as shown in Fig. 4B, suggesting that the molybdenum atom cannot be incorporated into the framework of SBA-15 by the impregnation method. It is also not observed in Fig. 4C for K/Mo-SBA-15 samples, which might be due to the addition of potassium covering the IR vibration peak of the Si–O–Mo bond.

UV-Raman spectroscopy is a powerful technique for the characterization of catalytic materials and has been widely used to characterize molecular sieves. Fig. 5 shows the UV-Raman spectra of the DHT Mo-SBA-15 and the IWI Mo/SBA-15 catalysts. For comparison, the Raman spectrum of SBA-15 is also included in Fig. 5A. The Raman bands at 500, 604, 810, and 978 cm^{-1} are observed on all samples. The bands at 500 and 604 cm^{-1} are assigned to the three- and four-silane rings, and the band at 810 cm^{-1} is ascribed to the siloxane linkage. The band at 978 cm^{-1} is associated with defect sites such as the surface silanol groups [3,24,25]. For the sample with a very low Mo content ($x = 0.1$), a weak band at 969 cm^{-1} is detected. With the increase in Mo content from $x = 0.1$ to $x = 12$, a shoulder band at 980–990 cm^{-1} is also discernable. The same phenomenon has been reported for the MoO_x/SiO_2 catalysts under dehydration [3,24]. The band around 980 cm^{-1} can be assigned to the stretching vibration of terminal Mo=O of highly dispersed MoO_x species, such as monomeric MoO_x moieties, whereas the band at 969 cm^{-1} may be ascribed to a highly dispersed surface molybdenum species with interaction with SiO_2 [3,26]. The absence of Mo–O–Mo stretching in these samples indicates that the DHT catalysts with Mo content $x \leqslant 12$ mainly contain highly dispersed MoO_x species. The UV-Raman spectra of Mo/SBA-15 samples are shown in Fig. 5B. For the sample with very low Mo content ($x = 0.1$), similar to the DHT catalysts, only the stretching

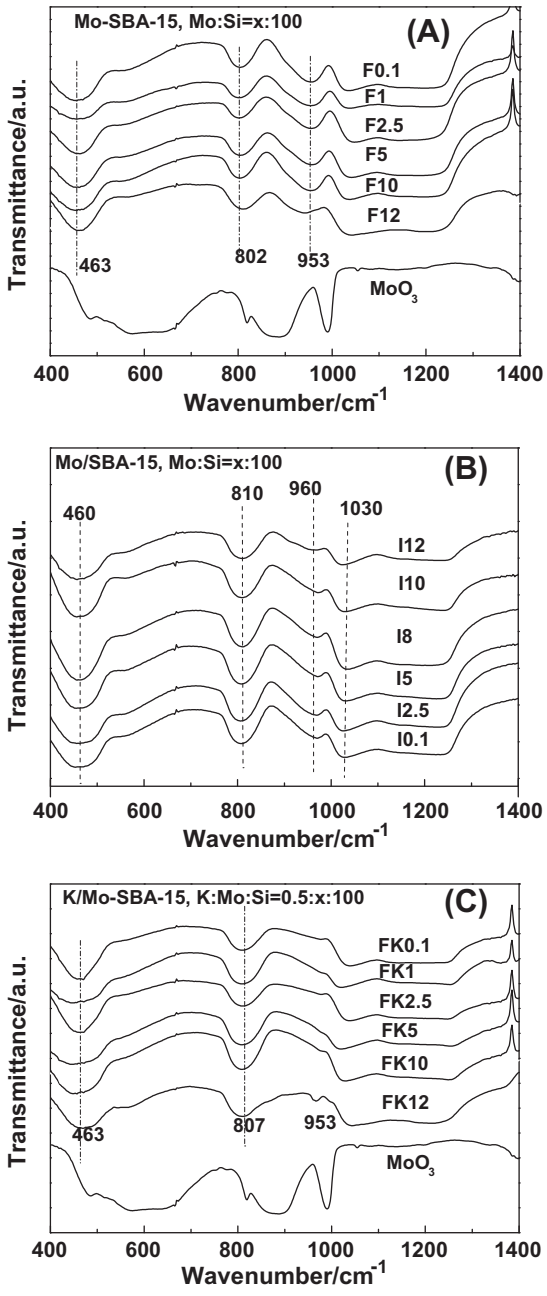

Fig. 4. FT-IR spectra of samples with different Mo contents. (A) Mo-SBA-15; (B) Mo/SBA-15; (C) K/Mo-SBA-15.

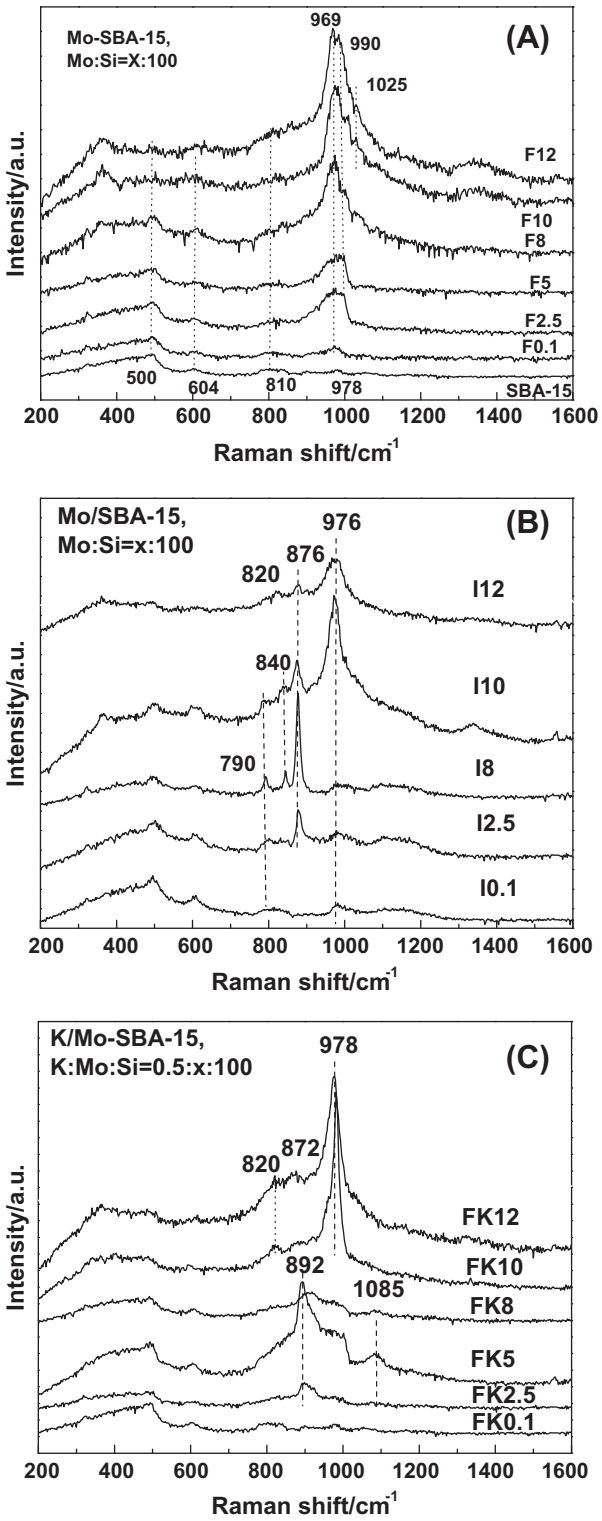

Fig. 5. Raman spectra of catalysts with different Mo contents. (A) Mo-SBA-15; (B) Mo/SBA-15; (C) K/Mo-SBA-15.

mode of terminal Mo=O of isolated momomeric MoO_x species centered at 976 cm^{-1} is observed, and no Mo–O–Mo stretching vibration of polymeric Mo species is detected. However, with increasing Mo content, the bands at 820–880 cm^{-1} corresponding to Mo–O–Mo stretching vibration of polymeric Mo species are observed even at low Mo content ($x = 2.5$). This means that Mo species in the IWI catalysts have more tendencies to aggregate than those in the DHT catalysts. As $x \geqslant 10$, the band at 976 cm^{-1} assigned to Mo=O stretching vibration becomes dominant. The coexistence of Mo=O and Mo—O—Mo bonds indicates that crystalline MoO_3 species are formed in the IWI catalysts at high Mo content ($x \geqslant 10$). Thus, UV-Raman results further indicate that the highly dispersed and isolated MoO_x species in high concentration were obtained in the Mo-SBA-15 catalysts by the framework-incorporation method but not in the Mo/SBA-15 catalysts by the incipient-wetness method.

Fig. 5C shows the UV-Raman spectra of K/Mo-SBA-15 samples. For the sample with very low Mo content ($x = 0.1$), no obvious difference is observed between K/Mo-SBA-15 and Mo-SBA-15. Besides the weak band at 969 cm^{-1}, another weak band at 980–990 cm^{-1} can also be discerned. When Mo content increases to $x = 2.5$ and $x = 5$, two new Raman peaks at 892 and 1085 cm^{-1} emerge, indicating the formation of potassium molybdate, and these two Raman peaks become weaker with further increase in

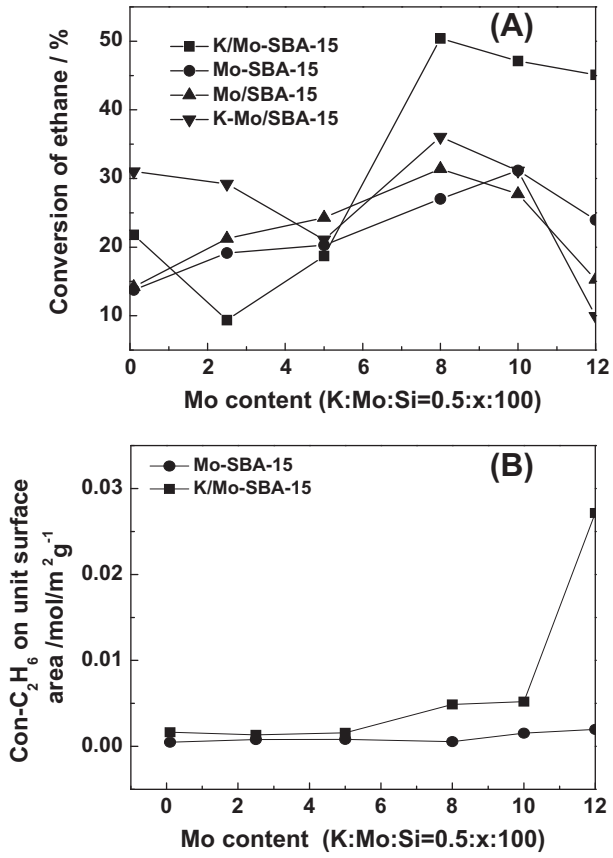

Fig. 6. (A) Ethane conversion over the four systems of Mo-SBA-15, Mo/SBA-15, K/Mo-SBA-15, and K-Mo/SBA-15 and (B) ethane conversion normalized to unit surface area over the Mo-SBA-15 and K/Mo-SBA-15 catalysts as a function of Mo content.

Mo content. The characteristic peaks of different potassium molybdates are at very similar or even the same frequencies [27], so it is very difficult to distinguish them. Several studies [27–30] have shown that some two-dimensional compounds without well-defined structures may be formed at low alkali metal content and at higher alkali metal content well-defined crystalline structures are more likely to form. Verbruggen et al. [27] studied alkali ion-modified silica-based Mo oxides and concluded that in the uncalcined samples with K/Mo $\leqslant$ 1, many sixfold-coordinated Mo species are present; mainly, $K_2Mo_2O_7$ is detected. At K/Mo > 1.0, the Mo coordination changes into fourfold, and mainly K_2MoO_4 is detected, which is differently distorted than in crystalline K_2MoO_4 [28]. Therefore, the observed changes in the Raman spectra of Fig. 5C can also be interpreted in terms of the MoO_x interaction with potassium to form potassium metal molybdates. The sharp peaks of the K/Mo-SBA-15 (K/Mo > 1, mol) at 892 and 1085 cm^{-1} may be ascribed to the formation of K_2MoO_4 [20,29], the isolated Mo species dominating the surface of the sample. When Mo content increases to $x = 10$ (K/Mo < 1, mol), several new Raman peaks at 820, 872, and 978 cm^{-1} are observed, indicating the formation of two-dimensional polymolybdates, which were probably ascribed to $K_2Mo_2O_7$ [19,30]. All results have shown that the presence of the alkali metal K modified the structure of the molybdenum oxide phase and formed new species of $K_2Mo_2O_7$ and K_2MoO_4.

3.2. Comparison of the catalytic performances of DHT and IWI catalysts

Fig. 6 displays the results of C_2H_6 conversion over different catalysts at 575 °C. As shown in Fig. 6A, in the absence of potassium, C_2H_6 conversion gradually increases with increasing Mo content, and it reaches a maximum at $x = 10$ for the DHT catalysts and $x = 8$ for the IWI catalysts, respectively. The addition of potassium has a complex effect on the ethane conversion. Table 3 also shows that a decrease in C_2H_6 conversion is observed for K/Mo-SBA-15 catalysts as Mo content changes from $x = 0.1$ to $x = 2.5$; it is remarkably enhanced with increasing Mo content and reaches a maximum value of 50.4% at $x = 8$, and then C_2H_6 conversion decreases slightly with a further increase in Mo content ($x = 10$ or 12). As shown in Fig. 6B, the ethane conversion normalized on unit surface area is constant for all Mo-SBA-15 catalysts, whereas it gradually increases with increasing Mo content for K/Mo-SBA-15 catalysts. A sharp increase in ethane conversion per unit surface area at $x = 12$ may be attributed to the severe reduction in the specific surface area of this catalyst (see Table 1).

Fig. 7 displays the yield of ethylene and acetaldehyde and the total yield of ethylene and acetaldehyde in the selective oxidation of C_2H_6 over different catalysts at 575 °C. In the absence of potassium, the yield of ethylene on the DHT catalysts is lower than that on the IWI catalysts when Mo content x is in the range $0.1 < x < 10$ (Fig. 7A). When $x > 10$, the yield of ethylene on the DHT catalyst is higher than that on the IWI catalyst. Furthermore, it decreases with the further increase in Mo content no matter whether it is on the DHT or on the IWI catalysts. The yield of acetaldehyde increases with the increasing Mo content at medium molybdenum content, as shown in Fig. 7B. Further increase in Mo content ($x \geqslant 10$) causes a decrease in the yield of acetaldehyde. When Mo content is low, the yield of acetaldehyde on the catalysts

Table 3
The catalytic performance of K/Mo-SBA-15 catalysts in the selection oxidation of ethane at 575 °C.

Sample	K:Mo:Si:molar ratio	*T*, °C	C_2H_6Conv., %	Selectivity, %						Selectivity, %
				CO_x[a]	Olefin[b]	Alkane[c]	Aldehydes			Olefins + aldehydes
							C1	C2	Total[d]	
FK0.1	0.5:0.0025:100	575	21.8	44.7	49.1	1.8	0.9	3.3	4.3	53.4
FK2.5	0.5:0.038: 100	575	9.4	29.5	64.5	2.1	2.7	1.1	3.8	68.3
FK5	0.5:0.045: 100	575	18.7	36.7	53.3	2.3	1.0	6.7	7.7	61.0
FK8	0.5:0.13: 100	575	50.4	32.2	43.0	7.3	0.5	16.9	17.4	60.4
FK10	0.5:1.85: 100	575	47.1	31.9	38.3	7.9	0.1	21.7	21.8	60.1
FK12	0.5:6.79: 100	575	45.1	39.4	45.0	6.4	1.6	7.1	8.9	53.9

Notes: C1: formaldehyde, C2: acetaldehyde. F is denoted as framework-incorporation sample Mo-SBA-15; I is denoted as incipient-wetness impregnation sample Mo/SBA-15; FK is denoted as the K/Mo-SBA-15 sample after potassium was impregnated on Mo-SBA-15; IK is denoted as the K-Mo/SBA-15 sample after potassium was further impregnated on Mo/SBA-15.

[a] CO_x: CO and CO_2.

[b] Olefins: ethylene, propylene, and butylene.

[c] Alkane: methane and propane.

[d] Total: formaldehyde, acetaldehyde, and acrolein.

is similar. When x is greater than 2.5, with the increased Mo content, the yield of acetaldehyde on the DHT catalysts is remarkably higher than that on the IWI catalysts, indicating that isolated Mo species favor the formation of acetaldehyde. The yield of ethylene greatly increases after the addition of potassium to the Mo-SBA-15 catalysts, as shown in Fig. 7A. Under the same reaction conditions, the maximum ethylene yield is only 8.9% for Mo-SBA-15 catalyst at $x = 8$. However, it reaches 19.9% after the addition of potassium at $x = 8$, and it is still very high at $x = 10$ (18.1%). In K/Mo-SBA-15 catalysts, the addition of potassium does not cause much enhancement in the yield of acetaldehyde when Mo content is low ($x = 0.1$, 2.5, and 5). As Mo content increases further, the yield increases remarkably after the addition of potassium. When Mo content is up to $x = 12$, yield decreases, as shown in Fig. 7B. When Mo content is low, the yield of acetaldehyde on the DHT or IWI catalysts is similar. With increasing Mo content, the yield of acetaldehyde on the DHT catalysts is much greater than that on the IWI catalysts. As shown in Fig. 7B, the maximal yield of acetaldehyde is 10.2% for K/Mo-SBA-15 catalyst at $x = 10$. As far as we know, this is the highest one-pass yield of acetaldehyde in the literature as yet for the selective oxidation of ethane to produce aldehyde oxygenates. Fig. 7C shows the total yield of acetaldehyde and ethylene over different systems of catalysts. The total yield is always greater on K/Mo-SBA-15 catalysts than on other three systems of catalysts with the same Mo content. Thus, it is very interesting to investigate the reaction kinetics for the selective oxidation of ethane onto K/Mo-SBA-15 catalysts.

Turnover frequency (TOF) is defined as number of ethane conversions per Mo site per second. Ethane conversion over Mo sites in a catalyst is determined by subtracting the conversion over pure SBA-15 from the total conversion over the catalyst. To calculate TOF values, the active sites should be identified and quantified; however, this is almost impossible even if dispersion data are available, because not all surface Mo atoms are equally active. Therefore, we use the "apparent TOF" to assess an "averaged" efficiency of Mo in different catalysts for catalyzing the reaction [31]. For incorporated/supported Mo oxide catalysts, the isolated/polymeric sites are known to be active sites and the number can be estimated based on the molybdenum loading. Fig. 8 shows the TOF as a function of the Mo content. A very high TOF is achieved on all catalysts when the Mo content of x is equal to 0.1. The decrease in TOF with increasing Mo content may be due to some structural modifications of the surface molybdenum species. It may indicate that the highly dispersed Mo on SBA-15 plays an important role in the oxidative conversion of ethane to acetaldehyde and ethylene. The addition of potassium into catalysts increases the TOF. The TOF value reaches a maximum at $x = 8$ for K/Mo-SBA-15 catalysts due to the formation of different potassium molybdates, further indicating that the selective oxidation of ethane is a structure-sensitive reaction.

To investigate the stability of catalysts, the effects of reaction time on ethane conversion and on product selectivity at 575 °C over K/Mo-SBA-15 (nominal molar ratio K:Mo:Si = 0.5:10:100) were also investigated. The results are depicted in Fig. 9. Only a small change is observed for the product distribution with time on stream. The conversion of ethane was maintained at 47%. At the same time, there was only a slight effect of the reaction time on the selectivity of ethylene, acetaldehyde, and Co_x, as shown in Fig. 9A. These results indicate that the catalyst was stable under the reaction conditions.

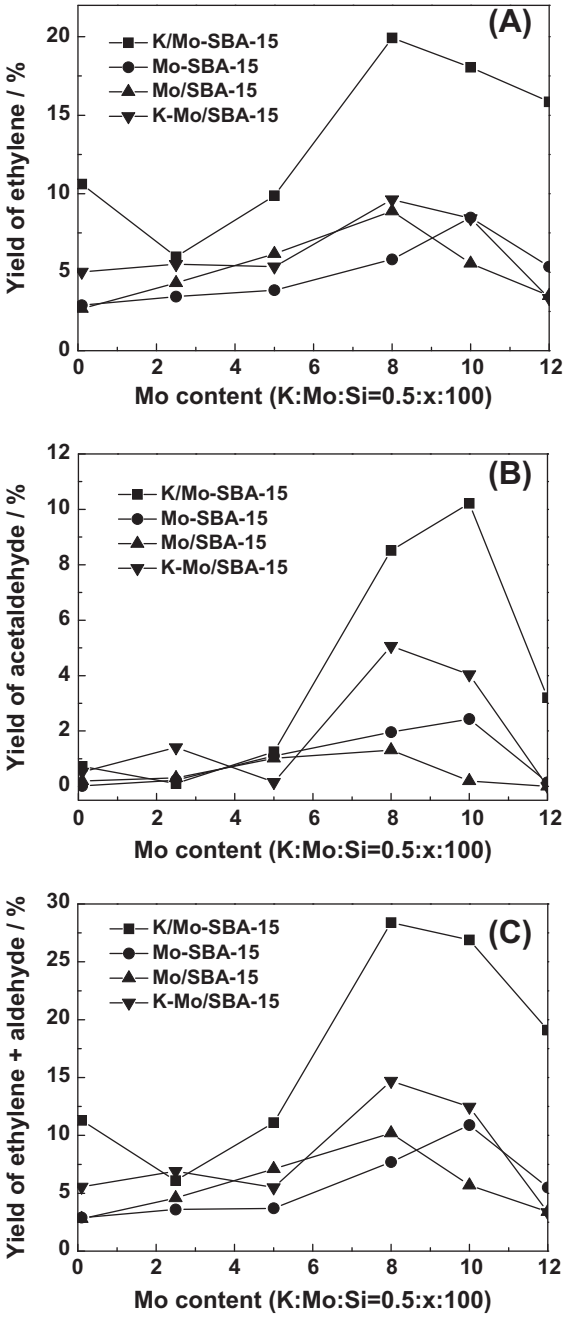

Fig. 7. Yield of ethylene and acetaldehyde over the four systems of Mo-SBA-15, Mo/SBA-15, K/Mo-SBA-15, and K-Mo/SBA-15 catalysts as a function of Mo content.

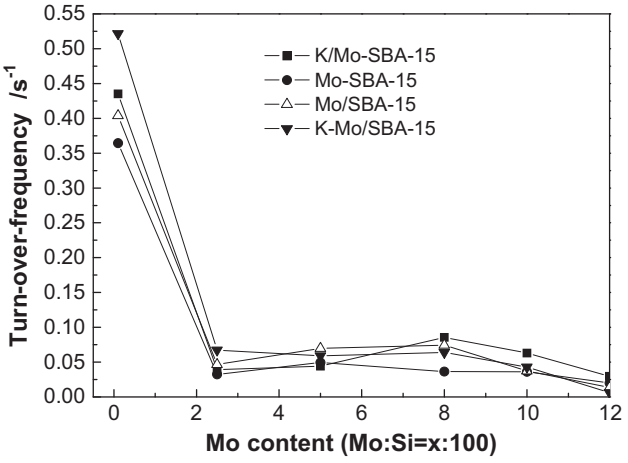

Fig. 8. TOF of ethane conversion over Mo-SBA-15, Mo/SBA-15, K/Mo-SBA-15, and K-Mo/SBA-15 catalysts as a function of Mo content.

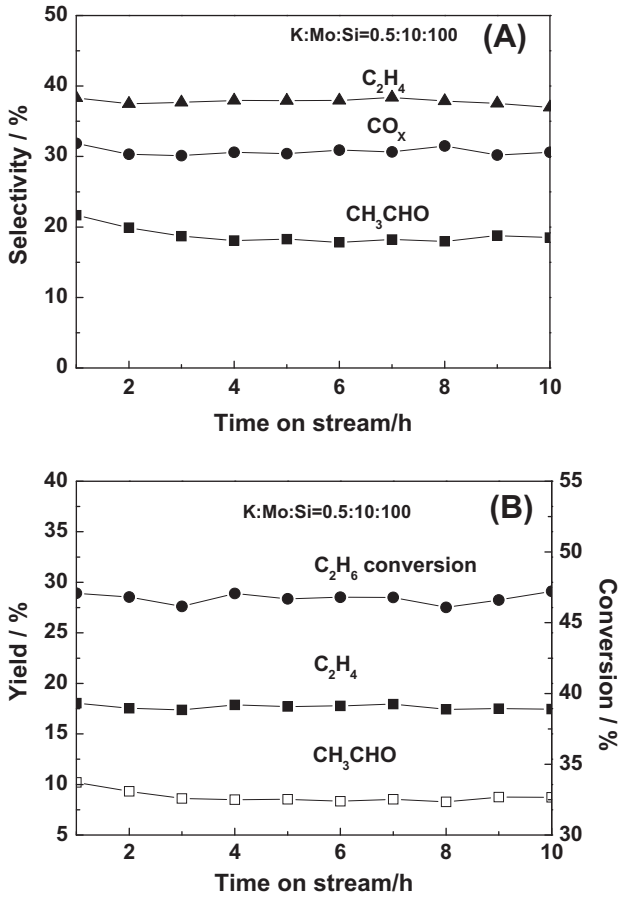

Fig. 9. Catalytic performance of K/Mo-SBA-15 catalysts (K:Mo::Si = 0.5:10:100) as a function of reaction time for the selectivity oxidation of ethane. Reaction conditions: W = 0.3 g, T = 575 °C, F = 900 ml/min, C_2H_6/O_2 = 3:1.

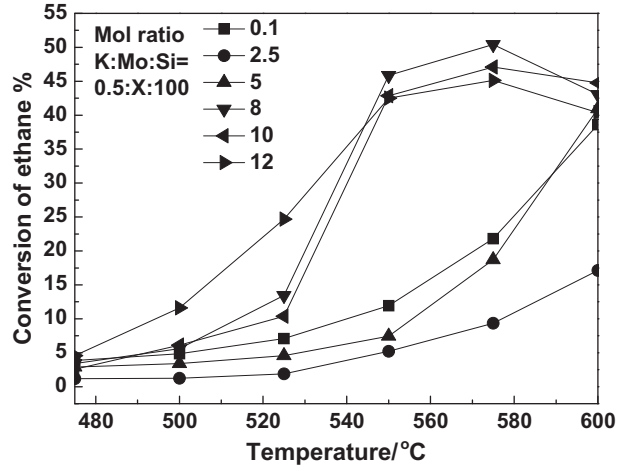

Fig. 10. Conversion of ethane as a function of reaction temperature over K/Mo-SBA-15 catalysts.

3.3. Kinetic investigation on the catalytic oxidation of ethane on the framework-incorporated K/Mo-SBA-15

3.3.1. Effect of temperature

The conversion of C_2H_6 as a function of temperature over K/Mo-SBA-15 catalysts at constant space velocity is illustrated in Fig. 10. For catalysts with different Mo contents, the conversion of ethane increases with increasing reaction temperature. The conversion of C_2H_6 changes little above 550 °C, and it even decreases slightly at 600 °C. Therefore, the best optimal temperature is 575 °C for the selective oxidation of ethane. The conversion of C_2H_6 reaches a maximum of 50.2% when the reaction temperature is 575 °C at x = 8.

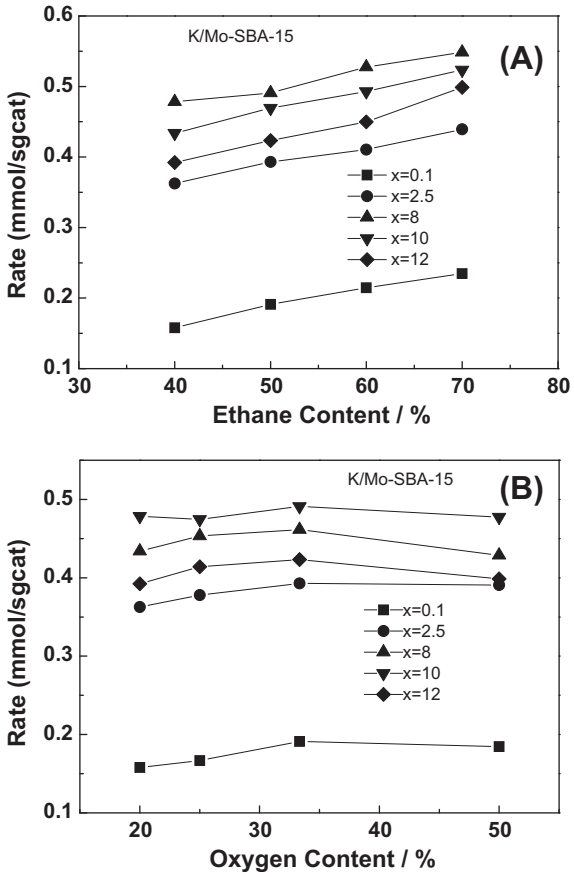

Fig. 11. Effect of ethane and oxygen content on ethane conversion rate over different K/Mo-SBA-15 catalysts.

3.3.2. Effect of reactant concentration on ethane oxidation

The rate of ethane consumption increases almost linearly with the increase in ethane concentration, as illustrated in Fig. 11A. However, the rate of C_2H_6 oxidation appears to be insensitive to O_2 concentration when oxygen content in reactant gases is 0.2–0.5, as can be observed in Fig. 11B. Kinetic data imply that the selective oxidation of ethane is approximately first order with respect to ethane and is consistent with a mechanism in which the breaking of a C—H bond is rate-determining. The reaction was found to be almost independent of the oxygen concentration, probably indicating that under reaction conditions, the reoxidation of reduced catalyst is not the rate-determining step, which is consistent with other reported results [32–34].

3.3.3. Effect of ethane or ethylene conversion on the selectivity of products

To elucidate the reaction network for ethane oxidation, the experiments were performed using different hydrocarbons as reactants, such as ethane or ethylene. The selectivity of products for the partial oxidation of ethane as a function of ethane conversion is illustrated in Fig. 12. As the ethane conversion increases, the selectivity of ethylene decreases, while the selectivity of CH_3CHO

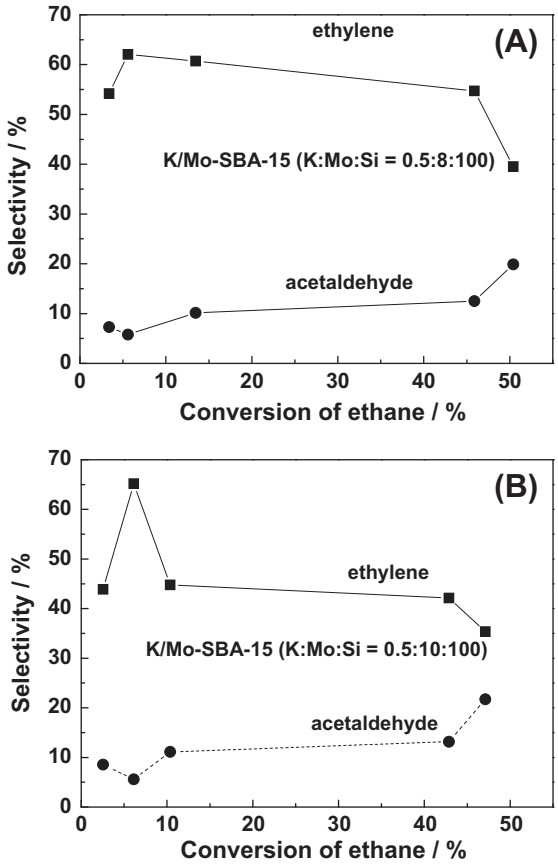

Fig. 12. Selectivity of ethylene and acetaldehyde as a function of ethane conversion over the typical K/Mo-SBA-15 catalysts (x = 8, 10).

increases at the expense of C_2H_4. This indicates that ethylene appears as the primary product of the partial oxidation of ethane. The main useful products at 575 °C for K/Mo-SBA-15 catalyst (with x = 8) are found to be ethylene and acetaldehyde, with selectivity of 39.5% and 19.9%, respectively. The decrease in ethylene selectivity with corresponding increase in acetaldehyde selectivity indicates that acetaldehyde is the secondary product of consecutive oxidation of ethylene. The selectivity and yield of products for the partial oxidation of ethylene or ethane over K/Mo-SBA-15 with x = 8 catalyst as a function of temperature are illustrated in Fig. 13. The selectivity and yield of acetaldehyde from ethylene are much greater than those from ethane. These results may further show that acetaldehyde originates directly from ethylene.

3.3.4. Reaction pathway for ethane oxidation

Study on the kinetics of selective oxidation of alkanes is helpful in obtaining important information about the reaction mechanism. Even though the kinetic studies cannot determine the molecular mechanism, they allow the exclusion of certain reaction pathways and help evaluate particular reaction routes and different catalytic sites in the proposed mechanism [32,35–37]. Three possible routes can be considered for the acetaldehyde formation: (1) direct oxidation of ethane, (2) ethanol as an intermediate, and (3) ethylene as an intermediate:

$$C_2H_6 \rightarrow CH_3CHO \quad (1)$$

$$C_2H_6 \rightarrow CH_3CH_2OH \rightarrow CH_3CHO \quad (2)$$

$$C_2H_6 \rightarrow C_2H_4 \rightarrow CH_3CHO \quad (3)$$

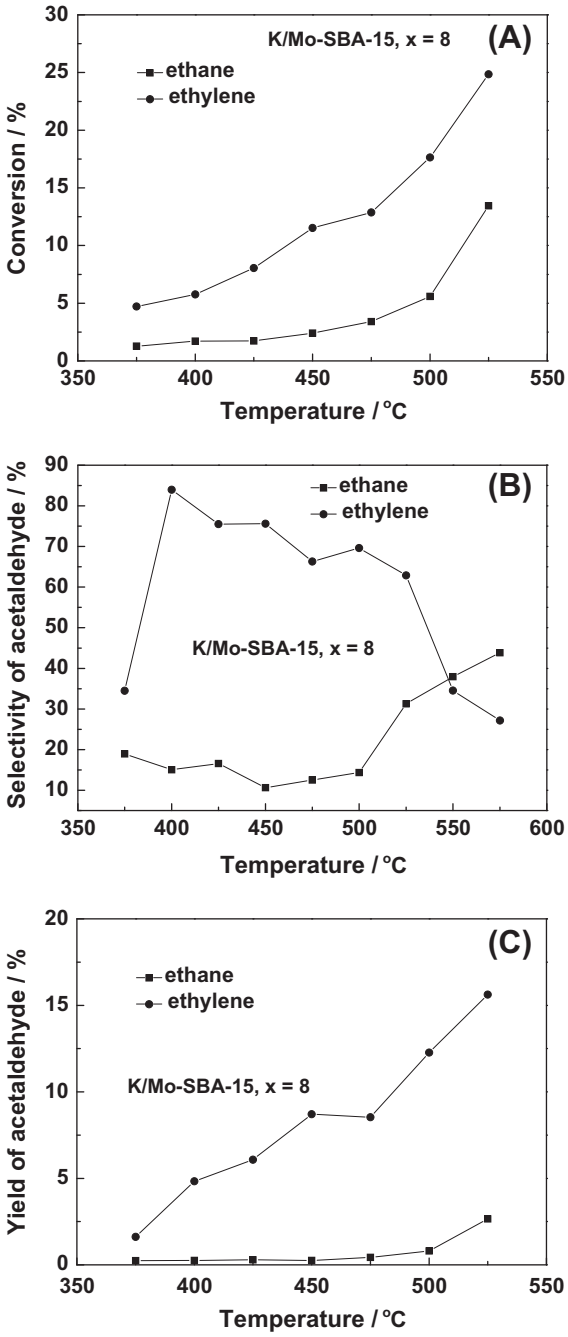

Fig. 13. (A) Conversion of ethylene and ethane (B) selectivity and (C) yield of acetaldehyde for partial oxidation over the typical K/Mo-SBA-15 catalyst (x = 8) as a function of reaction temperature.

No ethanol was detected in the ethane oxidation reactions over K/Mo-SBA-15 catalysts. Therefore, acetaldehyde formation via Eq. (2) can be excluded from possible reaction routes under these reaction conditions. This may suggest that CH_3CHO should be produced by the reaction pathways of Eqs. (1) and (3). The reactivity of ethane is much lower than that of ethylene, and the yield of acetaldehyde from ethane oxidation is also much lower than that from ethylene, as shown in Fig. 13. Therefore, it is not likely that acetaldehyde is mainly produced from the direct oxidation of ethane via Eq. (1).

The reaction scheme for ethane oxidation includes parallel reactions forming ethylene and acetaldehyde, and ethylene may be fur-

ther oxidized to acetaldehyde. Linke et al. reported that the consecutive reactions are favored at low temperatures [38]. Our results exhibit that ethylene as an intermediate in the consecutive reaction is favored at relatively high temperatures. This may be because the addition of potassium, which is favorable for the desorption of ethylene and acetaldehyde, mitigates the deep oxidation of ethane [12]. It is clear that the activation energy of the ethane oxidation to ethylene must be lower than the activation energy of the direct oxidation of ethane to acetaldehyde. CO_x is formed from ethane, ethylene, and acetaldehyde. In finding out which reaction is the rate-determining step in the oxidation of ethane, the following reasons are considered. Acetaldehyde desorption cannot be the rate-determining step, since different rates of acetaldehyde formation were found in ethylene and ethane oxidation. The results reveal as well that catalyst reoxidation is not the rate-determining step, since the oxygen content did not affect the ethane oxidation rate in ethane conversion. In addition, the lower ethane oxidation rate also suggests that the activation of the C—H activation in ethane, not the reoxidation of the catalyst, should be the rate-controlling step. This is because, if the latter applied, then similar rates of oxidation should be expected for both ethane and ethylene. Thus, the kinetic results are consistent with the activation of ethane being a rate-determining step in the overall oxidation of ethane. These preliminary kinetic results are consistent with the previous reports [3,35,38].

It is noted that the selectivity to acetaldehyde from ethane is lower than that from ethylene, as shown in Fig. 13B. This finding is in agreement with the previous reports about propane/propylene oxidation to acrylic acid [39]. It is known that the catalyst surface is more reduced in the oxidation of olefins than in that of alkanes, which must be linked to different selectivities [40,41]. The higher selectivity to acetaldehyde from the oxidation of ethylene than from that of ethane may be related to the difference in the existing states of Mo oxide species. The more easily reduced the Mo oxide species on the catalyst surface, the higher the selectivity to acetaldehyde.

4. Conclusions

In this work, framework-incorporated Mo-SBA-15 mesoporous molecular sieve catalysts with different Mo:Si molar ratios were successfully synthesized by a one-step hydrothermal method. They were further modified by potassium by the incipient-wetness impregnation method. The results show that highly ordered mesoporous structures of Mo-SBA-15 materials are formed with large surface area and uniform mesoporous structures. XRD, IR, and Raman results demonstrate that Mo ions are incorporated into the framework of SBA-15. For both DHT and IWI catalysts, the structural regularity of SBA-15-based mesoporous material decreases with increasing Mo content and is destroyed in the Mo-SBA-15 catalysts at $x = 12$. Meanwhile, the addition of potassium causes partial collapse of the mesoporous structure of K/Mo-SBA-15 (initial K:Mo:Si = 0.5:12:100).

Kinetic data suggest that the selective oxidation of ethane is approximately first order with respect to ethane concentration and that ethylene is a possible intermediate for acetaldehyde formation. The activation of ethane may be a rate-determining step in the overall oxidation of ethane.

The potassium-modified catalysts give supercatalytic performances for the selective oxidation of ethane to acetaldehyde. TOF values also increase in the presence of potassium. Among all catalysts, K/Mo-SBA-15 (initial K:Mo:Si = 0.5:10:100) catalyst gives the highest selectivity of $CH_3CHO + C_2H_4$ (68.3%) and the maximum yield of acetaldehyde (10.2%). This is the best result for the selective oxidation of ethane to acetaldehyde reported so far in the literature.

Acknowledgments

This work was supported by the National Natural Science Foundation of China (Nos. 20773163, 20833011, 20803093, 21173270, and 21177160), the Program for New Century Excellent Talents in the University of China (NCET-10-0811), the 863 Program of China (No. 2009AA06Z313), the Beijing Outstanding Ph.D. Thesis Foundation (No. YB 20091141401), a CNPC Project (2011D-4604-0101), the Innovation Foundation (2010D-5006-0402), and the Doctor Select Foundation (No. 200804251016).

Appendix A. Supplementary material

Supplementary data associated with this article can be found, in the online version, at doi:10.1016/j.jcat.2011.09.029.

References

[1] D.I. Enache, E. Bordes, A. Ensuque, F. Bozon-Verduraz, Appl. Catal. A 278 (2004) 103.
[2] Y. Wang, K. Otsuka, J. Catal. 171 (1997) 106.
[3] Y. Lou, H. Wang, Q. Zhang, Y. Wang, J. Catal. 247 (2007) 245.
[4] Z. Zhao, Y. Yamada, Y. Teng, A. Ueda, K. Nakagawa, T. Kobayashi, J. Catal. 190 (2000) 215.
[5] F. Wang, J. Dubois, W. Ueda, J. Catal. 268 (2009) 260.
[6] A. Erdohelyi, F. Solymosi, J. Catal. 123 (1990) 31.
[7] Z. Zhao, Y. Yusuke, A. Ueda, H. Sakurai, T. Kobayashi, Appl. Catal. A 196 (2000) 37.
[8] D. Vitry, J. Dubois, W. Ueda, J. Mol. Catal. A 220 (2004) 67.
[9] N. Haddad, E. Bordes-Richard, A. Barama, Catal. Today 142 (2009) 215.
[10] L.J. Huerta, P. Amorós, D. Beltrán-Porter, V.C. Corberán, Catal. Today 117 (2006) 180.
[11] Z. Zhao, Y. Yamada, A. Ueda, H. Sakurai, T. Kobayashi, Catal. Today 93–95 (2004) 163.
[12] Z. Zhao, J. Liu, C. Xu, A. Duan, T. Kobayashi, I.E. Wachs, Topics Catal. 38 (2006) 309.
[13] D. Zhao, J. Feng, Q. Hu, N. Melosh, G.H. Fredrickson, B.F. Chmelka, G.D. Stucky, Science 279 (1998) 548.
[14] J.Y. Ying, C.P. Mehnert, M.S. Wong, Angew. Chem. Int. Ed. 38 (1999) 56.
[15] Q. Zhang, Y. Wang, Y. Ohishi, T. Shishido, K. Takehira, J. Catal. 202 (2001) 308.
[16] J. Liu, Z. Zhao, C. Xu, A. Duan, G. Jiang, J. Phys. Chem. C 112 (2008) 5930.
[17] T. Kobayashi, Catal. Today 71 (2007) 69.
[18] R.B. Watson, U.S. Ozkan, J. Catal. 191 (2000) 12.
[19] K. Chen, S. Xie, A.T. Bell, E. Iglesia, J. Catal. 198 (2001) 2322.
[20] I.E. Wachs, Catal. Today 27 (1996) 437.
[21] H. Huang, C. Zhao, Y. Ji, R. Nie, P. Zhou, H. Zhang, J. Hazard. Mater. 178 (2010) 680.
[22] I. Eswaramoorthi, A.K. Dalai, Micropor. Mesopor. Mater. 93 (2006) 1.
[23] L.P. Wang, A.G. Kong, B. Chen, J. Mol. Catal. A 230 (2005) 143.
[24] H. Hu, I.E. Wachs, S.R. Bare, J. Phys. Chem. 99 (1995) 10897.
[25] X.T. Gao, S.R. Bare, B.M. Weckhuysen, M. Banares, I.E. Wachs, J. Phys. Chem. B 102 (1998) 10842.
[26] G. Tsilomelekis, A. Christodoulakis, S. Boghosian, Catal. Today 127 (2007) 139.
[27] N.F.D. Verbruggen, G. Mestl, L.M.J. Hippel, B. Lengeler, H. Knozinger, Langmuir 10 (1994) 3063.
[28] Z. Liu, Y. Chen, J. Catal. 177 (1998) 314.
[29] N.F.D. Verbruggen, L.M.J. Hippel, G. Mestl, B. Lengeler, H. Knozinger, Langmuir 10 (1994) 3073.
[30] R.S. Weber, J. Catal. 151 (1995) 470.
[31] A. Christodoulakis, S. Boghosian, J. Catal. 260 (2008) 178.
[32] F. Rahman, K.F. Loughlin, M.A. Al-Saleh, M.R. Saeed, N.M. Tukur, M.M. Hossain, K. Karim, A. Mamedov, Appl. Catal. A 375 (2010) 17.
[33] K. Ruth, R. Burch, R. Kieffer, J. Catal. 175 (1998) 27.
[34] M.D. Argyle, K. Chen, A.T. Bell, E. Iglesia, J. Phys. Chem. B 106 (2002) 5421.
[35] E. Heracleous, A.A. Lemonidou, J. Catal. 237 (2006) 175.
[36] F. Klose, M. Joshi, C. Hamela, A. Seidel-Morgenstern, Appl. Catal. A 260 (2006) 101.
[37] M. Machli, C. Boudouris, S. Gaab, J. Find, A.A. Lemonidou, J.A. Lercher, Catal. Today 112 (2006) 53.
[38] D. Linke, D. Wolf, M. Baerns, S. Zey, U. Dingerdissent, J. Catal. 205 (2002) 32.
[39] K. Chen, A. Khodakov, J. Yang, A.T. Bell, E. Iglesia, J. Catal. 186 (1999) 325.
[40] G. Centi, G. Fornasari, F. Trifio, J. Catal. 89 (1984) 44.
[41] B. Solsona, M.I. Vazquez, F. Ivars, A. Dejoz, P. Concepcion, J.M. Lopez Nieto, J. Catal. 252 (2007) 280.